European Journal of Pharmaceutics and Biopharmaceutics 138 (2019) 37–47

Contents lists available at ScienceDirect

European Journal of Pharmaceutics and Biopharmaceutics

journal homepage: www.elsevier.com/locate/ejpb

Research paper

Modeling of nanoparticle transport through the female reproductive tract for the treatment of infectious diseases

Lee B. Sims[a,1], Hunter A. Miller[b,1], Michael E. Halwes[a], Jill M. Steinbach-Rankins[a,b,c,d,2], Hermann B. Frieboes[a,b,e,*,2]

[a] Department of Bioengineering, University of Louisville, Louisville, KY, USA
[b] Department of Pharmacology and Toxicology, University of Louisville, Louisville, KY, USA
[c] Department of Microbiology and Immunology, University of Louisville, Louisville, KY, USA
[d] Center for Predictive Medicine, University of Louisville, Louisville, KY, USA
[e] James Graham Brown Cancer Center, University of Louisville, Louisville, KY, USA

ARTICLE INFO

Keywords:
Nanoparticles
Nanotherapy
3D cell culture
Sexually transmitted infections (STIs)
Female reproductive tract (FRT)
Intravaginal delivery
Mathematical modeling
Computational simulation

ABSTRACT

The secreted mucus layer in the vaginal epithelium presents a formidable barrier to the transport of active agents for the prevention and treatment of female reproductive tract (FRT) infections. Nanoparticle-mediated drug delivery has been proposed to help facilitate the transport and release of active agents through the cervicovaginal mucus (CVM) and underlying mucosa. However, both nanoparticles (NPs) and free active agents face a variety of challenges, often requiring the administration of high localized doses to circumvent leakage and poor penetration to targeted intravaginal tissue compartments. To address these challenges, "stealth" NP modifications have been investigated, due to their favorable mucus-penetrating properties, resulting in improved intravaginal active agent retention and transport. A number of other NP characteristics including size, surface modification type, ligand density, and co-modification, as well as the complexity of the FRT tissue are involved in obtaining adequate tissue penetration and, if needed, cell internalization. Studies that systematically investigate variations of these characteristics have yet to be conducted, with the goal to obtain a better understanding of what properties most impact prophylactic and therapeutic benefit. To complement the progress made with experimental evaluation of active agent transport in *in vitro* and *in vivo*, mathematical modeling has recently been applied to analyze the transport performance of agents and delivery vehicles in the FRT. Here, we build upon this work to simulate NP transport through mucus gel, epithelial, and stromal compartments, with the goal to provide a platform that can systematically evaluate transport based on NP and tissue characteristics. Model parameters such as PEG density and NP release (decay) rate from mucus gel into the epithelium, are set from previous *in vitro* and *in vivo* experimental work that assessed the transport of poly(lactic-co-glycolic acid (PLGA) NPs. The modeling results show that while unmodified and 2% PEG-modified NPs were retained in mucus for ~1–4 h, dependent upon decay constant values, and traverse to the epithelium, no NP penetration was observed in the stroma. In contrast, NPs modified with 3% PEG, exhibited prolonged retention in each compartment, remaining for ~4–6 h. Moreover, a significant concentration of NPs is observed in the stroma, indicating a transition in transport behavior. For NPs modified with 5, 8, or 25% PEG, steady retention profiles were noted, which gradually decline over 24 h. To supplement this modeling study and to develop a more representative experimental system that may be useful in future work, we report on the feasibility of constructing single and multicellular layered (MCL) culture systems to represent the epithelial and stromal tissue of the FRT. We anticipate that a combined mathematical/experimental approach may longer term enable prediction and customization of patient tissue-specific approaches to attain effective NP-mediated drug delivery and release for the treatment of infectious disease.

* Corresponding author at: Department of Bioengineering, Lutz Hall 419, University of Louisville, KY 40292, USA.
E-mail address: hbfrie01@louisville.edu (H.B. Frieboes).
[1] Equal contribution
[2] Joint senior authorship

https://doi.org/10.1016/j.ejpb.2018.09.003
Received 21 May 2018; Received in revised form 6 August 2018; Accepted 6 September 2018
Available online 07 September 2018
0939-6411/

1. Introduction

Mucosal barriers have a crucial role in preventing and retarding pathogen entry into the body. The effectiveness of the mucus layer in deterring pathogen invasion paradoxically presents a major obstacle to the delivery of therapeutic agents via oral (gastrointestinal tract), respiratory (nasal cavity and lungs), or topical (cervicovaginal) application [1–9]. In particular, the cervicovaginal mucosa (CVM) and underlying mucosa present a complex multi-layered environment (Fig. 1), with unique characteristics influencing the transport of therapeutic agents. The secreted mucus layer, which is apically located, consists of polymerized mucin fibers and globular secretions. Beneath this layer is the stratified epithelium which is approximately 200–400 μm thick, while the lamina propria (or stroma) lies basally and is the thickest layer (2.5–3 mm), containing immune (CD4 +) and host (macrophage) cells. A vast array of mucin fibers can also be found within the stroma [1]. The arrangement of these fibers, as an aligned or randomized fiber meshwork, is influenced by menstrual and ovulation cycles.

Various drug delivery platforms have been devised to maintain active agent stability and intravaginally deliver effective doses, while minimizing adverse effects. For delivery to the female reproductive tract (FRT), a multitude of platforms have been developed to provide sustained-release [9–16]. Yet mucin fibers in the apical and basal portions of the CVM present a significant barrier to the diffusive transport of active agents and drug delivery vehicles [4,17]. Depending on the mucin fiber arrangement, pores of varying sizes may impede or facilitate agent or vehicle passage. Additionally, the affinity of delivery platforms to reversibly bind to mucin fibers has proven to be a key factor affecting diffusive transport. In addition to transport barriers, vaginal retention and clearance rates impact delivery vehicle and active agent localization. Vehicles that superficially bind to the luminal mucus layers are rapidly cleared and thus unable to penetrate the underlying adherent mucus and mucosal tissue layers [17,18]. However, molecules that exhibit mucoadhesive properties or are able to rapidly penetrate through the luminal mucus layer can improve retention [18].

Active agents encapsulated in nanoparticles (NPs) have been explored as a means to overcome intravaginal delivery barriers, in part due to the simplicity with which their physicochemical properties can be tuned to attain desired pharmacokinetic (PK) and pharmacodynamic (PD) properties.[18–24] For topical intravaginal delivery, surface modification via the addition of ligands can either enhance NP diffusion through vaginal mucus and the mucosa [4,6,17,21,25] or impart mucoadhesive properties [26,27], thereby enhancing retention within the FRT. In particular, Polymeric NPs have proven to be highly effective in this regard [5,10,28], with *in vitro* and *in vivo* experiments providing insight into how diffusive transport through cervicovaginal mucus is dependent on ligand choice, surface density, and molecular weight.

However, the design of NPs and their modifications to effectively penetrate and elicit prophylactic or therapeutic effect in the CVM is nontrivial, primarily due to the multitude of NP characteristics and biological factors involved. As such, iterative testing of all potential NP design and tissue conditions is infeasible. To complement the experimental effort, mathematical modeling and computational simulation have been recently applied to provide a more systematic evaluation of efficacy, transport, and potential design tradeoffs for intravaginal delivery [1,9]. Mathematical modeling can provide insight into the PK and PD properties of molecules and drug delivery platforms, especially as a function of diffusion and distribution through physiological environments that are difficult to evaluate experimentally. This modeling may serve as a tool to test variations of different system parameters, and to identify molecule and drug delivery platform formulations that may be efficacious in clinical application.

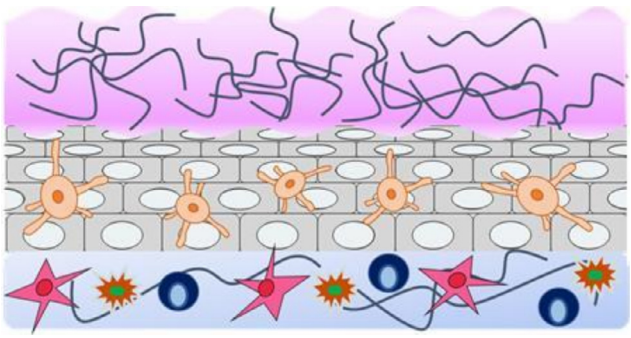

Fig. 1. Schematic structure of the CVM showing the mucus gel (top), epithelium (middle), and stromal layers (bottom).

Previous modeling effort has primarily focused on studying the diffusion of small molecules through the CVM and underlying mucosa after release from a topically applied gel, intravaginal ring, or film [1–9]. Yet there remains a critical need to evaluate NP-mediated agent delivery to the FRT, as the impact of factors such as NP size, surface modification type, ligand density, and co-modification on diffusive transport, remain poorly understood. Although there are additional mechanisms of molecule transport through the mucosa – such as receptor mediated transcytosis [29] – passive diffusion, both paracellular and transcellular, prevails as the predominant transport mechanism [30,31]. Accordingly, this study focuses on the diffusive flux of NPs, as this has been modeled in both vaginal tissue and experimental systems that recapitulate *in vivo* results. Furthermore, microbicide modeling studies have shown that diffusive flux is the main mechanism used to simulate transport of drug molecules in the FRT [1,32–34].

Building upon previous work modeling the transport of antiretroviral drugs in the FRT [1,9], here we develop a framework to simulate NP performance in terms of diffusive transport and distribution through the CVM. We describe a multi-compartmental model that incorporates first-order reaction rate constants and measurable parameters based on NP physicochemical properties that have been shown to significantly impact diffusive transport. Some of the parameters of interest include NP release rate from the mucus gel (decay rate) and PEG modification density, as functions of tissue compartment (i.e., mucus gel, epithelium, or stroma) and time. As a first step, these parameters are set from previous *in vitro* and *in vivo* experimental work evaluating poly(lactic co-glycolic acid) (PLGA) NPs in monolayer cell cultures and in murine models, respectively. By developing a mathematical model that accurately predicts NP diffusion as a function of these critical parameters, we aim to establish the feasibility of a framework to systematically assess variation in NP characteristics, including different ligand types, densities, and co-modifications. Further, to provide for a more detailed experimental evaluation of diffusive transport and measurement of associated model parameters in the future, we explore the feasibility of constructing single and multicellular layered (MCL) cell culture systems to represent CVM tissue *in vitro*. With further refinement, these culture systems may provide an experimental set-up that helps to overcome the limitations of monolayer culture, while avoiding the complications of *in vivo* systems. Longer term, the determination of therapeutic parameters, including NP surface modifications, via a combined mathematical/experimental approach that is customized to patient-specific FRT conditions, may achieve the goal of effective active agent delivery through the CVM.

2. Methods

2.1. Mathematical model

Mathematical modeling has been previously applied in the field of intravaginal and microbicide delivery to evaluate the PK and PD and often cytotoxic behavior of various small molecules and therapeutic agents. In particular, mass balance driven models have been developed [1,2], with the CVM and mucosal layers represented as distinct compartments, thus providing for the capability to evaluate diffusive

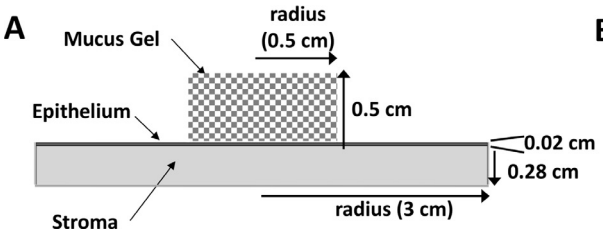

Fig. 2. Schematic representation of the vaginal epithelium dimensions used to model nanoparticle release from mucus gel in the CVM. (A) System cross-section. The model simulates a single compartment of gel from which nanoparticles diffuse, following the model in [35]. The compartment representing the mucus gel is 0.5 cm thick and has a radius of 0.5 cm. The radii of the epithelial and stromal compartments are both 3 cm, while the thicknesses of the epithelium and stroma are 0.02 cm and 0.28 cm, respectively (shown to scale). (B) 3D representation of the modeled vaginal epithelium.

transport through each layer. The models are comprised of partial differential equations which account for the diffusive flux of small molecules, as well as their clearance within each compartment [1,2].

2.1.1. Transport model

We build upon this previous work [1,2] to represent the complex process of NP diffusion through the three main layers of the FRT (Fig. 2), represented here in a layered concentric schematic as follows: a 0.5 cm × 0.5 cm disk for the mucus gel (top), a 3 cm × 0.02 cm disk for the vaginal epithelium (middle), and a 3 cm × 0.28 cm disk for the vaginal stroma (bottom), respectively denoting disk radius × height. The model implements three mass balance equations to account for the NP transport through each of these layers, as follows:

$$\frac{\partial C_m}{\partial t} = D_m \nabla^2 C_m - (k_m + k_a + k_{bd}) C_m \quad (1)$$

$$\frac{\partial C_E}{\partial t} = D_E \nabla^2 C_E - k_a C_E \quad (2)$$

$$\frac{\partial C_S}{\partial t} = D_S \nabla^2 C_S - (k_b + k_a + k_{bd}) C_S \quad (3)$$

These equations govern the mass transport of NPs through the secreted mucus gel (Eq. (1), the squamous epithelium (Eq. (2) and the stroma (Eq. (3). Variable C represents the NP concentration within each compartment: mucus gel (m); epithelium (E); and stroma (S). NP diffusivity within each layer is represented by D. To account for physiological and physicochemical factors affecting the PK/PD behavior of surface-modified NPs, reaction rate parameters are defined as summarized in Table 1.

Three parameters are defined to account for critical NP physicochemical parameters that may significantly affect diffusive transport. In Eq. (1), k_m is a first-order reaction rate constant characterizing the clearance of NPs from the mucus gel compartment due to vaginal fluid and secretions, while k_b in Eq. (3) is the first-order clearance term representing the loss of NPs to the vascular and lymphatic system below the stromal layer. In both of these equations, the rate k_{bd} characterizes the affinity for NPs to reversibly bind to and unbind from the mucin fibers, as the mucin fiber meshwork is only found within the secreted mucus and stromal layers of the FRT. This reversible binding is dependent on the NP surface properties, and has been shown to affect NP diffusion due to transport hindrance via binding and obstruction by mucus pores. In all equations, the rate constant k_a characterizes the probability of the NPs to self-aggregate. If the average diameter of this aggregate exceeds that of the mucin fiber pore size or becomes too large to transcytose through the epithelium, then the NP transport will be hindered or halted [4,6,10,17].

Table 1
Mathematical model reaction rate parameters.

Parameter	Definition	References
k_m	NP clearance due to vaginal fluid	[21]
k_{bd}	NP reversible binding to mucin	[6,10]
k_a	NP self-aggregation	[6]
k_b	NP clearance to vascular and lymphatic systems	[21]

2.1.2. Transport model initial conditions

At the initial time of treatment ($t = 0$) the NP concentration in the mucus gel compartment is assumed equal to an initial concentration C_0 (Eq. (4), while the concentrations in the epithelial and stromal compartments are null (Eqs. (5) and (6). Steady-state conditions are assumed at time equal to infinity (Eq. (7).

$$C_m = C_0, \quad t = 0 \quad (4)$$

$$C_E = 0, \quad t = 0 \quad (5)$$

$$C_S = 0, \quad t = 0 \quad (6)$$

$$\frac{dC}{dt} = 0, \quad t = \infty \quad (7)$$

2.1.3. Transport model boundary conditions

No flux boundary conditions are applied to the lumen/mucus gel (Eq. (8) and to the stroma/vasculature (Eq. (9) interfaces. Since the model domain represents a theoretical tissue cross-section, transfer boundary conditions are assumed at the (lateral) sides of the geometry (Eqs. (10) and (11), with q denoting the transfer coefficient out of the region (assumed to be equivalent to the lateral diffusion coefficient of the NPs in the region that contains the boundary).

$$\frac{\partial C_m}{\partial x} = 0, \quad x = \text{lumen/mucosal layer interface} \quad (8)$$

$$\frac{\partial C_S}{\partial x} = 0, \quad x = \text{stroma/vasculature layer interface} \quad (9)$$

$$\frac{\partial C_E}{\partial x} = qC_E, \quad x = \text{lateral edge of epithelial region} \quad (10)$$

$$\frac{\partial C_S}{\partial x} = qC_S, \quad x = \text{lateral edge of stromal region} \quad (11)$$

The release of NPs from the gel into the mucus compartment is assumed to follow a simple decay function $C_0 e^{-Bt}$. The decay rate constant B was varied over a 3-fold order of magnitude from 0.001 to 1, with the latter case representing an upper bound on the same order as that of drug molecules eluting from a fibrous mesh [35]. A representation of the overall system geometry and the associated boundary conditions are depicted in Fig. 3.

2.1.4. Numerical solution

The MATLAB Partial Differential Equation Toolbox was used to solve the system of differential equations (Mathworks. MATLAB. 7.11.0 ed. MathWorks Inc.: Natick, MA; 2010). The solution builds upon recent work that simulated the transport of Tenofovir released from PLGA fibers in the FRT [35]. The mesh for the domain consisted of approximately 48,000 triangular elements.

2.2. In vitro systems

With the goal to obtain a more detailed measurement of NP

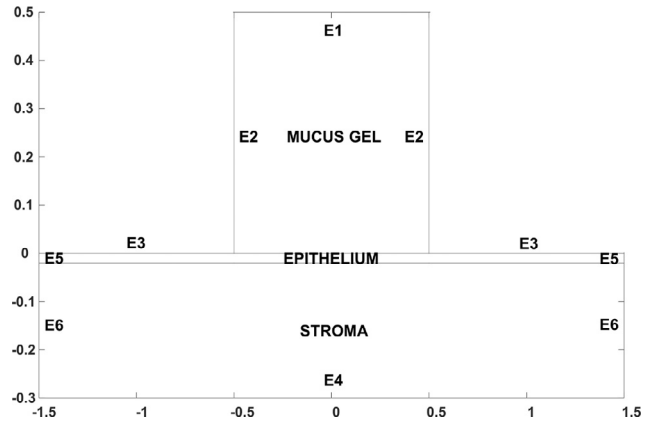

Fig. 3. Representation of the system geometry in simulated tissue. No flux boundary conditions were applied along edges E1, E2, and E3. The solution was held to be zero at the bottom of the stroma, represented by edge E4. Transfer boundary conditions were applied along edges E5 (flow out of the epithelium) and edges E6 (flow out of the stroma). Units are in cm.

diffusive transport and associated model parameters via *in vitro* systems in the future, we assessed the feasibility of constructing cellular models that represent squamous and columnar epithelial tissue. These included multicellular layers (MCL) with SiHa cervical cancer cells and single cell layers with VK2/E6E7 vaginal epithelial cells.

2.2.1. Multicellular layer formation

The cervical carcinoma cell line SiHa was initially used to validate the growth of stratified epithelium *in vitro* [36]. Prior to cell seeding, transwell inserts were coated with 100 µL of collagen (Type 1 from rat tail, Sigma C3867) solution diluted in 70% EtOH to a final concentration of 800 ng/mL. Inserts were dried in a sterile cell culture hood for 6 h prior to cell addition, to allow for EtOH evaporation. After the drying period, SiHa cells that had reached 70% confluence were passaged and seeded onto transwell inserts with a polyester membrane (Corning 3472), at a density of 1×10^6 cells per well per 100 µL. Additionally, 700 µL of culture medium was added to the basal well, ensuring that the insert was fully submerged in a total volume of 800 µL. The transwell plates were subsequently incubated in 37 °C, 5% CO_2 and allowed to grow overnight (24 h). To enable viable expansion of these multilayer cultures, 470 mL culture jars were sterilized and prepared for subsequent incubation. After sterilization, 70 mL MEM (supplemented with 10% FBS and 1% P/S) media and a micro-stir bar were added to each jar. Following the initial 24 h growth period, inserts were removed from the plates and positioned in foam flotation cutouts to allow inserts to freely float in the jars. The insert + flotation device was carefully placed in the culture jar using sterile tweezers. Culture jars containing cell inserts were placed on a stir plate set to approximately 200 rpm and allowed to grow for 7 days under normal cell culture conditions.

2.2.2. Multicellular layer imaging

Following the 7 day growth period, inserts were removed from the culture jars for processing. Briefly, the insert membrane containing the MCL was carefully cut to avoid damage to the MCL, and completely embedded in cryomolds containing Tissue-Tek® OCT compound. The inserts were frozen using dry ice, and the MCL was subsequently cryosectioned using a cryostat (LEICA CM1900) at a thickness of 20 µm. The sections were thaw-mounted onto Superfrost® Plus glass slides. Prior to immunocytochemistry staining, slides were dried at RT overnight and subsequently fixed with 300 µL of 4% paraformaldehyde for 10 min at RT. Following fixation, the MCL sections were stained with Texas Red Phalloidin (actin detection, 1:40 stock dilution) and Hoechst 33,342 (nuclei detection, 1 µg/mL) solutions. Lastly, slides were mounted with Vectashield hardening medium and stored at 4 °C prior to fluorescence imaging.

2.2.3. Single cell layer formation

Cell layers representing the healthy vaginal epithelium were used as an *in vitro* model [13,37,38] to assess NP transport. The vaginal cell line VK2/E6E7 was maintained in keratinocyte serum free medium supplemented with 0.1 ng/ml human recombinant epidermal growth factor, 0.05 mg/ml bovine pituitary extract, and additional calcium chloride 44.1 mg/L (ATCC). Once cells reached 70–80% confluency, they were seeded in 24-well cell culture inserts containing a polycarbonate membrane with a pore size of 5 µm (Corning 3421). Cells were seeded at a density of 5×10^4 cells/200 µL medium per insert, with 700 µL medium in the basal compartment of the well. Inserts containing cells were grown for six days after seeding to allow for cellular tight junction formation. Transepithelial electrical resistance (TEER) was monitored every two days by a volt-ohm meter to assess cell layer integrity and validate intercellular junction formation; values were normalized to an untreated cell culture insert control. After six days, cell layers were confirmed to have reached $\sim 30\,\Omega * cm^2$, indicating the presence of an intact, confluent cell layer [36–38], subsequently used for the transport experiments.

2.3. Nanoparticle experiments

2.3.1. NP synthesis

Ultra-small PLGA NPs encapsulating the fluorophore Nile Red were synthesized using an adapted oil-in-water (o/w) single emulsion technique, to enable visualization via fluorescence microscopy [39,40]. Ultra-small NPs (~70 nm), versus the typically sized ~150 nm NPs, were fabricated in these experiments due to the known transport dependence on size. Carboxyl-terminated poly(lactic co-glycolic acid, PLGA) (0.55–0.75 dL/g, LACTEL®) was used to synthesize 100–200 mg NP batches. Nile red was dissolved in methylene chloride (DCM) overnight at a concentration of 2 µg per mg of PLGA. The following day, the PLGA/Nile Red/DCM solution was added dropwise to a 5% polyvinyl alcohol (PVA) solution of equal volume, vortexed and sonicated. The resulting NPs were hardened in 0.3% PVA during solvent evaporation for 3 h. The NP/PVA suspension was centrifuged at 13,000 rpm for 10 min, followed by subsequent centrifugation of the supernatant at 100,000 × *g* to separate small (~150 nm NPs) from ultra-small (~70 nm) NPs.

The emulsion method was adapted to synthesize PEG-modified (5000 Da, Nanocs Inc.) NPs as described previously [16,39,40], Briefly, NPs were synthesized by adding an equal volume of avidin-palmitate (1 mg/mL) to the 5% PVA solution to obtain a total amount of 5 mg avidin/100 mg NP. Surface-modified NPs were collected after the first wash, and incubated for 30 min on a rotator with biotinylated ligands at a molar ratio of 3:1 ligand:avidin in PBS. Following this conjugation, PEG-modified NPs were washed and centrifuged at 100,000 × *g* as described above.

2.3.2. NP transport

Confluent VK2 cell layers were used as vaginal tissue mimics to evaluate NP diffusivity. Ultra-small PEG-modified and unmodified NPs were administered at an initial concentration of 100 µg/mL. At specified time points post-administration (1, 2, 4, 6, 24, 48 h), media in the basal compartment of the transwell system was collected and replenished with fresh media. The concentration of NPs at each time was determined using a fluorescence spectrophotometer with excitation/emission wavelengths of 550/630 nm, and compared to a known standard. To account for steric hindrance of NP diffusion through the insert membranes, the transport data were normalized to the quantity of unimpeded NPs, when transport was assessed in inserts alone without cells. NP transport was assessed in cell layers for both particle groups (n = 3).

VK2 layers were assessed (n = 3) for viability with TEER prior to NP administration. Each NP control and experimental group was tested in triplicate. An untreated cell layer was used as a control to continuously monitor TEER values throughout the NP treatment, and to confirm no loss in cell layer integrity. As noted above, VK2 layers were only used after confirming that TEER values were a minimum of 28 Ω * cm^2.

3. Results

3.1. Calculation of model parameters

The mathematical model parameters (Table 1) were estimated from previously reported values in the literature. Diffusivities D were obtained from experimental data by Xu et al. [6] for NPs modified with 5 kDa PEG at 0, 2, 3, 5, 8, 10 and 25% PEG densities. In that study, the diffusivity of fluorescently-labeled PEG-modified NPs in fresh, undiluted human vaginal mucus was measured as a mean squared displacement by single particle tracking. The average effective diffusivity was used to derive the diffusivity D for each particle type in our model. The rate of NP clearance k_m due to vaginal fluid leakage was estimated from [21], where the nanoparticle leakage on absorbent paper was measured 0.5 and 2 h after intravaginal administration of 750 μg of nanoparticles in a murine model. The leakage was measured in terms of mass, and the value of k_m was calculated by dividing the average NP quantity recovered in μg over a period of 0.5 h and dividing by the total mass of administered NPs. The rate of NP self-aggregation k_a was obtained from [6], for which the size distribution of (0, 2, 3, 5, 8, 10 and 25%) PEG-modified NPs was measured with respect to time in 10 mg/mL mucin (here, non-dimensionalized by the NP diameter). The value of k_a was calculated by taking the average size distribution across all incubation periods (ranging from 0 to 180 min) and dividing by the individual particle diameter. The NP clearance to the vascular and lymphatic systems k_b was set to 0 based on observations in [21]. The reversible binding of NPs to mucin k_{bd} was calculated from [6], which measured the amount of bound mucin per NP surface area (mg mucin/m^2) using isothermal titration calorimetry, and which was here non-dimensionalized by NP surface area divided by the initial mass of mucin. The mass was calculated by multiplying the concentration of mucin (2.2 mg/mL) by the calorimetric cell volume (1.4 mL). A rate was obtained by dividing the amount of bound mucin to NP surface area by the 2 h incubation period for the isothermal titration calorimetry technique [10]. These experimentally-derived parameter values are summarized in Table 2.

3.2. Simulation of NP diffusive transport

Next, the diffusive transport of NPs surface-modified with different PEG densities was simulated (Fig. 4), where the decrease in NP concentration is representative of the diffusion of NPs out of each compartment, in addition to their loss from the compartment. The initial mass of administered NPs was modeled using a value of 0.01 mg, to match our experimental data in which 10 μg NPs were administered in a volume of 100 μL media (100 μg/mL). Similarly, an initial mass of 0.05 mg in a volume of 5 μL (10 mg/mL), matching the murine data of [6] was also evaluated, yielding essentially the same transport behavior as the case with 0.01 mg, except that the corresponding magnitudes of concentration were increased 5-fold (data not shown).

One of the parameters of interest in this study was the effect of NP release rate from the mucus to surrounding tissue compartments. These values can vary, as shown in [6,10,21], and are known to significantly impact NP diffusion and distribution throughout the cervicovaginal mucus and underlying mucosa. From our modeling results, we observed that the maximum NP concentrations in each compartment increased as the NP decay rate, or release of NPs from the mucus gel compartment, decreased. Within the first hour after administration, the resulting concentration of NPs varied across a wide range for decay rate constants spanning three orders of magnitude (1–0.001 h^{-1}), respectively (Table 3).

For each decay constant value, as the % PEG-modification increased, the NP concentration in each compartment (mucus gel, epithelium, stroma) was generally higher with respect to time. The most prolonged NP retention was observed for the 0.001 decay constant, after 24 h resulting in concentrations of 4.7×10^{-5}, 1.2×10^{-5} and 5.8×10^{-6} μg/mL in the mucus, epithelium, and stroma, respectively. Furthermore, NPs with 3% or less PEG-modification density, demonstrated a sharp decline in concentration over the first 6 h, whereas NPs modified with 5, 8, or 25% PEG, evinced more gradual decreases in NP concentration. In all cases, the 5% PEG formulation maintained the highest concentrations across compartments. The rapid penetration and distribution of PLGA NPs into the vaginal tissue is consistent with previous experimental results *in vivo* [20]. In particular, PEG-modified PLGA NPs were readily detectable in mouse vaginal stroma 6 h post administration [21], with the NPs having at least an order-of-magnitude decrease in concentration over 24 h.

Overall, the simulations show that NP concentrations achieved in the mucus gel, epithelium, and stroma were similar for NPs with greater than 5% PEG modification, with all compartments retaining high concentrations of NPs, differing by an approximate order of magnitude, for at least 6 h. In contrast, NPs with less PEG modification and the most rapid decay constant of 1, demonstrated decreased NP concentration by an order of magnitude in the mucus gel and epithelium within 2 h. Similar, but more elevated trends were observed for the lowest decay constant 0.0001. In contrast in the stroma, unmodified or 2% PEG-modified NPs resulted in no NP penetration regardless of decay constant value. In these two NP groups, the decay constant had the strongest impact, particularly in achieving distribution to the underlying epithelium. These results highlight the strong dependence that NP retention and distribution have on surface modification, particularly at low surface ligand density, with a lesser, but still significant dependence on decay rate.

To quantify these observations, the AUC for each NP formulation was calculated as a function of PEG density, shown in Fig. 5. The results show that as the decay constant from the mucus gel to the epithelial compartment decreases, the AUC in each compartment increases. The 5% PEG formulation achieved the highest AUC in each compartment, followed by the 25% PEG-modified NPs. The values for the 10% PEG modification were the same as for the 25%, as expected based on their similar parameter values (Table 2), and are therefore not shown. To

Table 2
Mathematical model parameters calculated for NPs modified with 5 kDa PEG, at various PEG-modification densities.

% PEG density on NP surface	D (μm^2/s) (from [6])	k_m (1/s) (from [21])	k_a (1/s) (from [6])	k_{bd} (1/s) (from [6])	k_b (1/s) (from [10,21])
0	2.37×10^{-5}	73.33×10^{-5}	2.22×10^{-3}	7.28×10^{-18}	0
2	7.49×10^{-5}	18.5×10^{-6}	2.19×10^{-3}	2.32×10^{-18}	0
3	0.422	18.5×10^{-6}	6.53×10^{-4}	2.15×10^{-18}	0
5	0.237	18.5×10^{-6}	2.83×10^{-5}	7.88×10^{-19}	0
8	0.562	18.5×10^{-6}	0	7.55×10^{-19}	0
10	0.422	18.5×10^{-6}	0	7.68×10^{-19}	0
25	0.422	18.5×10^{-6}	0	2.91×10^{-19}	0

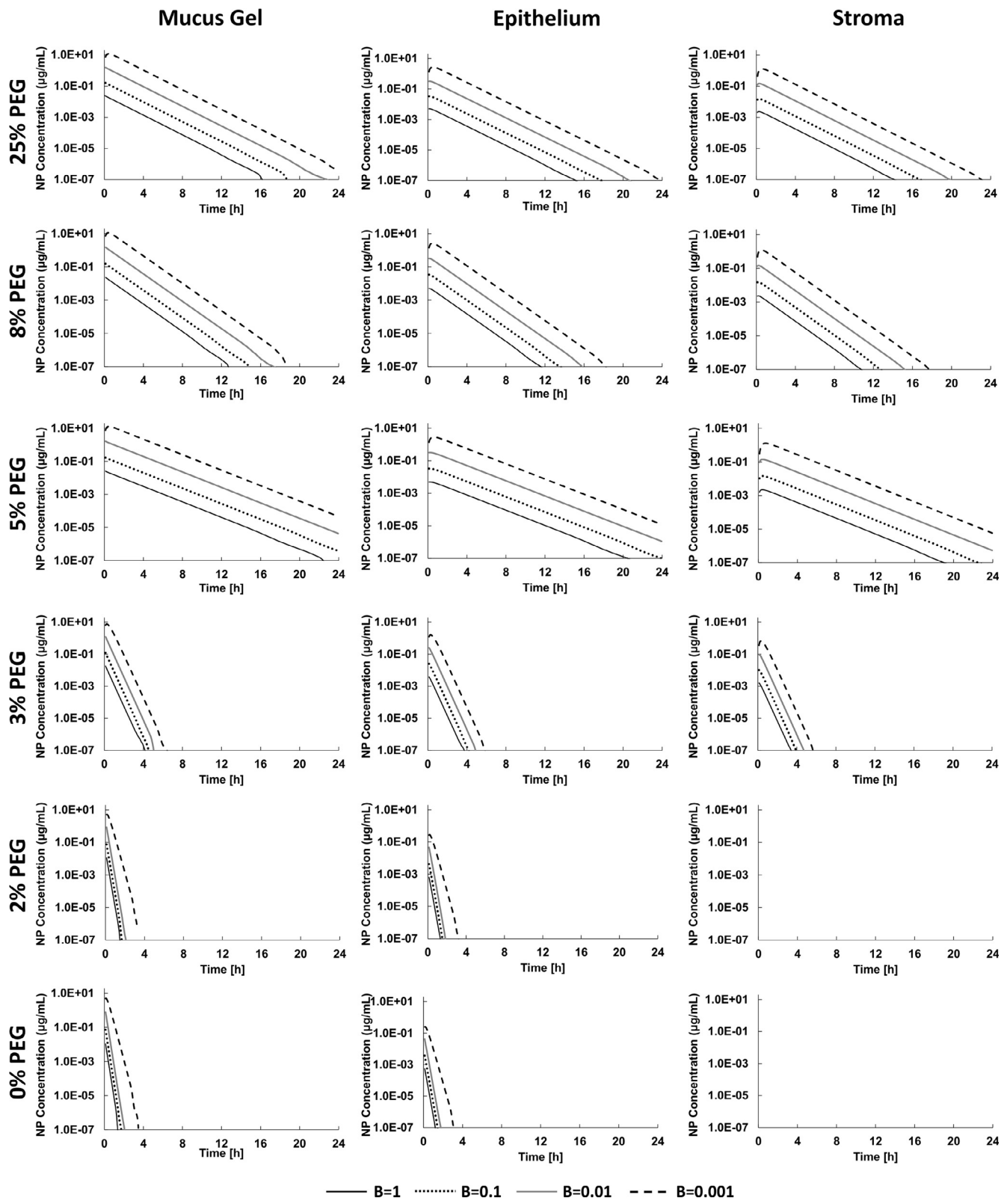

Fig. 4. Model-simulated penetration of PLGA NPs into the CVM, related as a function of NP concentration with respect to time, for various % PEG modifications, an administered dose of 0.01 mg (100 µg/mL), and a range of decay values from the mucus gel to the epithelial compartment (B = 1 through B = 0.001).

further validate the dependence of NP retention and transport on PEG modification density, the AUC value in each compartment for each % PEG formulation, as a proportion of the total AUC for the three compartments modeled in the mucus gel, epithelium, and stroma, is presented in Fig. 6. For PEG modifications of 3% or higher, the respective AUCs remain similar in each compartment, whereas for lower % PEG formulations, most of the NPs remained in the mucus gel, with negligible quantities of NPs transported into the epithelium and none into the stroma. The proportions transported were the same for all values of NP decay rates from the mucus gel into the epithelium.

Table 3
Concentration of NPs in each compartment at 1 h post administration, based on simulating variation in % PEG-modification and value of decay rate constant B from the mucus gel compartment.

% PEG density on NP surface	NP Concentration (μg/mL)											
	$B = 1\,h^{-1}$			$B = 0.1\,h^{-1}$			$B = 0.01\,h^{-1}$			$B = 0.001\,h^{-1}$		
	Mucus	Gel	Stroma	Mucus	Gel	Stroma	Mucus	Gel	Stroma	Mucus	Gel	Stroma
0	6.0×10^{-6}	4.7×10^{-7}	0	4.1×10^{-5}	3.2×10^{-6}	0	4.7×10^{-4}	3.6×10^{-5}	0	1.6×10^{-1}	9.1×10^{-3}	0
2	8.7×10^{-6}	8.2×10^{-7}	0	5.5×10^{-5}	5.3×10^{-6}	0	6.2×10^{-4}	5.9×10^{-5}	0	1.8×10^{-1}	1.2×10^{-2}	0
3	1.1×10^{-3}	2.8×10^{-4}	1.4×10^{-4}	7.5×10^{-3}	1.9×10^{-3}	9.2×10^{-4}	7.6×10^{-2}	1.9×10^{-2}	9.3×10^{-3}	1.6	3.9×10^{-1}	1.8×10^{-1}
5	1.5×10^{-2}	3.7×10^{-3}	1.8×10^{-3}	1.0×10^{-1}	2.5×10^{-2}	1.2×10^{-2}	9.7×10^{-1}	2.4×10^{-1}	1.1×10^{-1}	10.6	2.6	1.2
8	9.9×10^{-3}	2.5×10^{-3}	1.2×10^{-3}	6.6×10^{-2}	1.7×10^{-2}	8.1×10^{-3}	6.4×10^{-1}	1.6×10^{-1}	7.8×10^{-2}	7.6	1.9	9.2×10^{-1}
25	1.2×10^{-2}	3.1×10^{-3}	1.5×10^{-3}	8.3×10^{-2}	2.1×10^{-2}	1.0×10^{-2}	8.0×10^{-1}	2.0×10^{-1}	9.8×10^{-2}	9.1	2.3	1.1

3.3. Nanoparticle characterization

Verification of NP morphology was carried out via SEM, and size analysis was confirmed with ImageJ image processing. Both regular and ultra-small NPs exhibited spherical morphologies. Ultra-small NP size was compared to our typically formulated NPs, with unhydrated diameters of 66.3 ± 22 and 178.5 ± 45–nm, respectively.

3.4. Evaluation of CVM tissue mimics

To explore the feasibility of relating and assessing the impact of diffusive transport and measurement of associated model parameters in a more complex cell system, single and multicellular layer (MCL) cultures were fabricated. SiHa cells formed MCLs approximately 100 μm thick, while VK2 cells formed single-cell layers, approximately 10 μm thick. Prior to and during the transport experiments, VK2 cell layers were assessed for cell layer integrity. Visual confirmation using transmitted light microscopy indicated no change in cell layer structure or integrity after the growth period and during subsequent NP treatment. In addition TEER values remained at or above $28\,\Omega * cm^2$ for the duration of the experiments.

A representative MCL composed of SiHa cells is shown in Fig. 7, indicating potential usefulness as a squamous tissue architecture to inform NP design. In our study, NP penetration through these layers was found to be negligible at time points earlier than 6 h, suggesting that significantly longer times may be required to achieve NP penetration into the epithelium.

For a representative vaginal epithelium culture, the diffusive transport of unmodified and 5 kDa PEG-modified ultra-small NPs (~70 nm) was evaluated for 72 h with VK2/E6E7 cells in single-cell layers (Fig. 8). Both ultra-small unmodified and PEG-modified NPs demonstrated comparable penetration patterns, suggesting that the transport was not diffusion limited. As compared with a simple test case run with unmodified and PEG-modified NPs, it was observed that NPs continued to traverse cell layers at later time points.

4. Discussion

This study presents a simple multi-compartmental model to help evaluate the effect of polymeric NP modifications on diffusive transport through the FRT. The design of effective NP-mediated drug delivery for topical intravaginal delivery in the treatment of infectious disease critically depends on these modifications in order to successfully confront the mucosal barrier. A purely empirical effort is precluded by the physiological complexity of the mucus and underlying mucosa, and the variety of available approaches to design drug delivery vehicles that penetrate the mucus and target specific layers of the mucosa. Hence, mathematical modeling that can evaluate the transport behavior of varying NP formulations is expected to provide a powerful platform to guide experimental effort and maximize potential NP penetration. In this study, we take a first step towards this goal by constructing a model with parameters measured from previous experimental data (Table 1), building a system that predicts NP transport as a function of surface modification density and release rate from the mucus layer.

One of the most impactful alterations that has been investigated to improve NP transport through the FRT, is NP surface modification. To date, multiple studies have assessed the impact of NPs modified with a variety of PEG densities, to better traverse mucus and epithelial layers [6,18,22,25,38,41–45]. A significant number of these studies have been conducted via *in vitro* experiments [5,7,15,17,25], and select formulations have progressed for evaluation in the murine reproductive tract [6,21,43]. However, for applications in which NPs may be targeted to different mucosal layers, with a variety of modifications that enable cell targeting, uptake, or transport, it is critical to obtain a better understanding of the effect of specific modifications on transport through tissue.

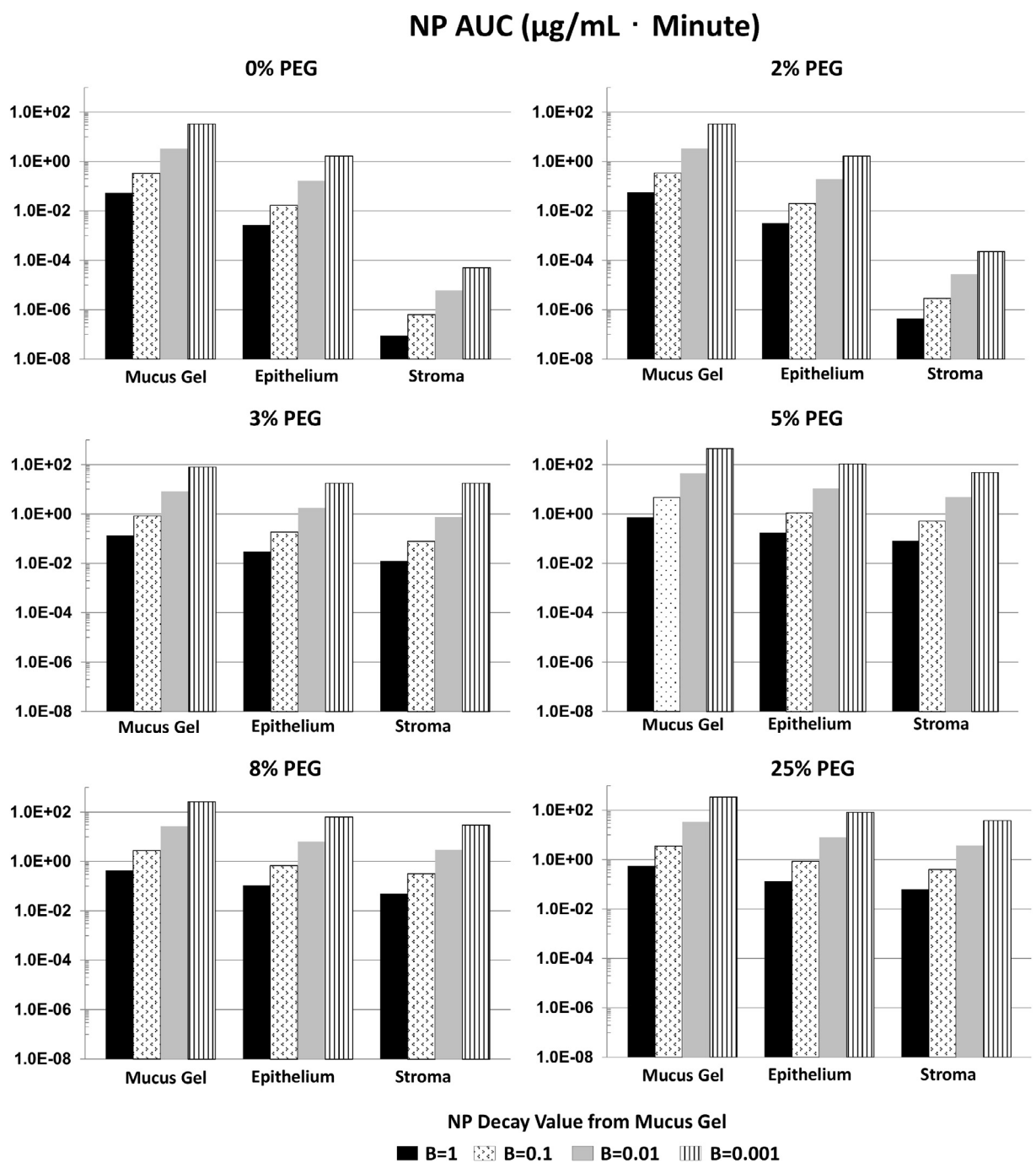

Fig. 5. Area-under-the-curve (AUC, in units of µg/mL · Minute) calculated for each compartment for PLGA NPs with various % PEG modifications and with a range of decay values (B = 1 to B = 0.001) from the mucus gel to the epithelial compartment.

With this in mind, we utilized previously published data from *in vitro* and *in vivo* experiments [6,10,21] to estimate parameter values and developed a model building upon previous work [1,2] to assess the diffusive transport of NPs as a function of NP physicochemical properties (here, surface modification) and clearance rate from the apical mucus layer (Fig. 2). Variations in PEG surface density were chosen as PEG has proven to be the most effective "stealth" ligand to achieve mucus penetration [5,6,8,17,25,39,46–49]. Hence, a higher density of PEG modification was expected to increase mucus penetration, due in part to the hydrophilicity of PEG, providing NPs with a diffusive flux in mucus comparable to that of water. Furthermore, PEG modification increases NP colloidal stability, which deters NP aggregation, thereby increasing the ability to diffuse between mucin fibers [5,6,8,17,25,39,46–49]. Based on previous *in vitro* and *in vivo* studies, a 5 kDa MW PEG molecule was modeled as it has demonstrated enhanced NP diffusion, relative to surface modification with higher MW PEG. Moreover, due to these favorable properties, to date, the most commonly studied NP modification in terms of transport has been PEG, with studies demonstrating the impact of PEG density and MW on diffusion. Given this, we selected PEG modification as the basis to build a model that can validate and predict the impact of surface modifications. While experimental studies have assessed these impacts, there are no predictive tools available to help non-iteratively refine the design of NP modifications (PEG or other) to understand their impact on transport. We anticipate that this model may be tailored in future work to not only consider PEG, but also to estimate the transport properties of other

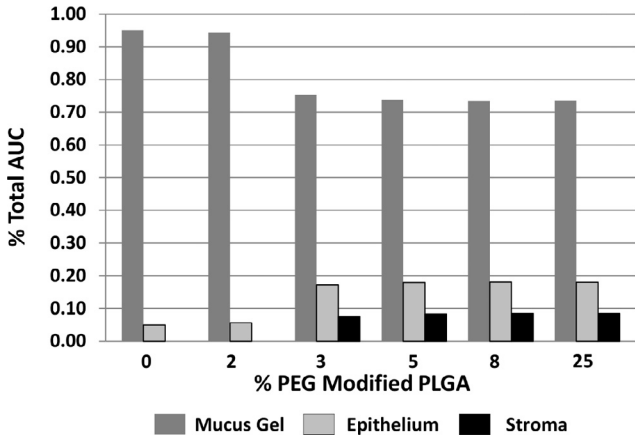

Fig. 6. Area-under-the-curve (AUC) values in each compartment for each % PEG formulation, as a proportion of the total AUC for the three compartments modeled in the CVM. The proportions were the same for all values of decay rate of NPs from the mucus gel into the epithelium.

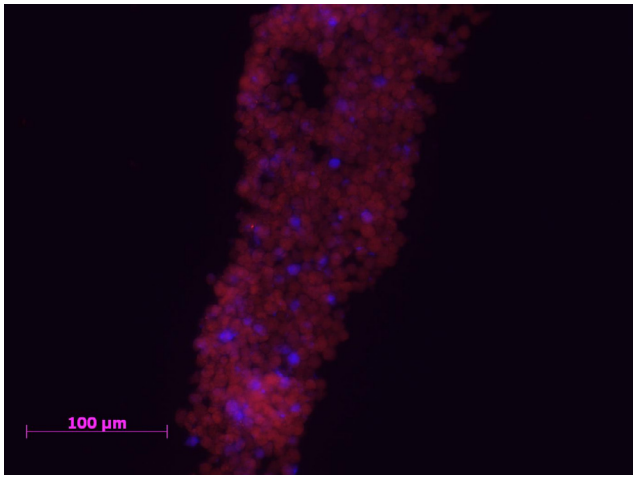

Fig. 7. Multicellular layer of SiHa cervical cancer cells growing in 3D cell culture *in vitro*. Staining is shown in red (Texas Red phalloidin) for actin filaments and in blue (Hoechst) for cell nuclei.

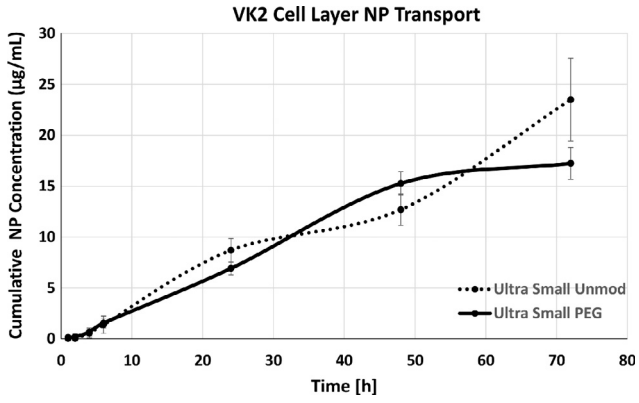

Fig. 8. Measurement of ultra-small unmodified and PEG-modified NP transport through VK2/E6E7 cell layers.

surface-conjugated molecules and more complex co-modifications.

To evaluate the effect of NP properties on transport, reaction constants that characterize the specific physicochemical properties of surface-modified NPs were considered in the mathematical model. The rate at which NPs self-aggregate and bind to mucin fibers is sensitive to NP surface properties and can thus be tailored using surface modification. The addition of these NP parameters expands the model's ability to evaluate how transport might change as a function of NP surface modification. This allows for a more descriptive platform to provide insight into how NP surface modification can contribute and affect diffusion in the cervical mucus and underlying mucosa.

The two main parameters assessed in this study were PEG modification density and the decay constant, representing NP release from the mucus gel into the epithelium. For the set of parameter values used here, the results show that unmodified and 2% PEG-modified NPs are retained in mucus for ~1–4 h, dependent upon decay constant and traverse to the epithelium, but no NP diffusion is observed in the stroma (Fig. 4). In comparison, NPs modified with 3% PEG, exhibit slightly prolonged retention in each compartment (mucus gel, epithelium), remaining for ~4–6 h, dependent upon decay constant. Moreover, a significant concentration of NPs is observed in the stroma, indicating a transition in transport behavior. Last, for NPs modified with 5, 8, or 25% PEG, steady retention profiles are noted, that gradually decline over the course of 24 h, dependent in overall magnitude on the decay constant. These results indicate that there may be a threshold value that will increase retention in the mucus, and, indeed, studies have observed that at a threshold density, PEG can enable mucoadhesive vs. mucoinert properties [25,43,50]. However, for these higher % PEG modifications, NPs penetrate the epithelium to reach the stroma in high concentration (Fig. 5).

These model-based observations with the given set of parameter values have important ramifications for NP design, in that if the delivery of an entry inhibitor is desired, versus a molecule that targets infected epithelial or stromal cells, different modification densities may impact efficacy more potently. In another sense, NP delivery as a prophylactic is often viewed as a "race" to prevent virus infection. Hence NP transport in the immediate time frame of the first few hours surrounding infection is critical to ensure that active agent reaches the target destination. These target destinations may vary, including the mucus/epithelium for general entry inhibitors or HSV-2 inhibition, or the epithelium and stroma for antiretroviral agents against HIV-1. The results shown here reinforce the need to predict and validate NP transport behaviors in the early time frames surrounding infection.

As compared with a simple *in vitro* test case run with unmodified and PEG-modified NPs, we observed in the experiments that at later time points the NPs continue to traverse cell layers, even in a simple single layer system (Fig. 8). Single layer culture systems may be useful to represent single columnar epithelial layers present in the endocervix, while multicellular models may represent squamous cell layers in the ectocervix and vagina. The continuation of NP release in our simple single cell layer set-up indicates that the model may not fully capture what is occurring at later time points. It should be noted, however, that cellular assays that utilize transwell set-ups may be convenient for assessing drug transport, but that limitations exist with NPs [37,51].

In this work, we utilized ultra-small NPs (~70 nm) to achieve diffusion through both single cell layers and empty transwell control membranes. In initial experiments utilizing typically sized PLGA NPs (~150 nm), very low penetration through the transwell inserts alone (both polyester and polycarbonate) resulted. This indicates that regardless of culture system on the membranes, size and hydrophobic interactions with the membrane may confound the experiment, as also observed in [37,51].

Additionally, some of the *in vitro* methods used to obtain empirical NP transport data obtained, either from the cell layer models described here or from other studies [6], may not accurately recapitulate the complex physiology of the FRT, and thus could impact the transport parameter values estimated in the model. The *in vitro* methods used here must be validated with results from *in vivo* or *ex vivo* studies, while in parallel exploring other cell culture models to obtain more reproducible, multilayered systems. Moreover, we recognize that mucus is not integrated in our *in vitro* cell culture, hence an additional barrier

layer is not present. This difference may partially account for the ability of NPs to continue penetrating the cell culture layer, while the simulations predict declining concentrations, regardless of parameter settings. These more complex multi-layered systems will be evaluated in future work. Last, the *in vitro* model was validated with NPs modified with only one density of surface ligand. In future work, we plan to expand upon this experimental work to assess and confirm the impact of different densities and ligand types on diffusion.

In addition to the mathematical model observations based on PEG density, the release of NPs from the mucus layer, as represented by the decay constant, had a major impact on NP distribution and concentration. Overall, as the decay rate constant decreased, NP concentration increased by an approximate order of magnitude in each compartment, for each modification type (Fig. 4). Despite null concentrations of NPs in the stroma for the unmodified and 2% PEG-modified NP formulations, this trend was generally observed regardless of modification density. The correlation observed between decay constant and initial/final concentrations in the various compartments over 24 h represents an important consideration for NP delivery, and is consistent with experimental data [7,18,24].

One of the primary challenges with NP delivery is the propensity for leakage from the mucus [21], as leakage from the FRT is dependent on the type of dosage form and the associated surface properties. This has been assessed using a variety of NP formulations, and rapid clearance from the superficial mucus layers remains a consistently encountered limitation [18,22]. This suggests the importance of better understanding the kinetics of mucoadhesive systems, and if this “decay rate” may be tailored, via surface modification or other methods (e.g. osmolarity of solution [15,52]), significant increases in delivery might be obtained. Moreover, variation of this decay constant offers insight into the impact that NP retention has in distribution in the mucus, and ubiquitously across compartments, and how important it is to keep NPs in the mucus during the first few hours surrounding delivery. Moreover, this parameter can be used in future work to estimate the impact of more adhesive (PEG can also be mucoadhesive) or charged ligands that are retained in mucus longer. Conversely, there may be a threshold at which the decay constant has a deleterious effect, inducing NP retention in the mucus, but restricted transport to other compartments.

In addition to the ability to vary ligand modification density and mucus removal rate, some of the modeling features that would be beneficial to build into this platform include the effects of non-stealth (non-PEG), receptor targeted, and cell penetrating NPs. Correspondingly, the effect of different modification densities of this variety of ligands on transport would be interesting to compare across different ligand types. Additionally, many studies have assessed multifunctional NPs that are co-modified with 2 or more ligands [39,40,53–59]. However, these NPs are often iteratively designed, making it challenging to assess more than a few logical variants of modification combinations and densities. Having the ability to better understand the molecular impact of co-modified NPs and even NP co-treatment groups [39,40], would provide some perspective as to how useful these co-modifications truly are, and how they can be designed to maximize efficacy. Moreover, for other molecules that enable cell targeting or penetration, the ability to tailor the model to incorporate the effects of ligand MW, and calibrating with *in vitro* or *in vivo* experiments would offer opportunities to understand how these platforms may perform *in vivo*. In addition, obtaining a better understanding of how changes in NP dose affect accumulation, clearance, and transport would be sound to relate to safety studies. In particular, having the ability to ascertain if there is benefit attained from the administration of a higher dose to increase localized concentration would provide much needed information for pre-clinical safety and efficacy studies. Lastly, the ability to incorporate other parameters, such as osmolarity of the administration solution could be highly impactful, as administration conditions have been shown to markedly affect intravaginal distribution [15,52].

In conclusion, a tool to systematically evaluate how NP surface modifications might significantly affect diffusion through mucus and tissue barriers may be beneficial when designing NP formulations for intravaginal delivery. The model presented here is offered as a first step for a better understanding of how changing the surface properties of NPs can either increase or retard diffusion and transport through the CVM, epithelial, and stromal compartments. When rationally designing NP delivery platforms, the goal for this model will be to both predict and understand how surface modifications can be used to tailor the pharmacokinetic and pharmacodynamics behavior of NPs to attain either mucoadhesive or mucus penetrating platforms, with the goal to overcome transport barriers and achieve efficacious drug-based prevention and treatment of infections in the FRT.

Acknowledgments

This work was partially supported by the Knight’s Templar Eye Foundation (for LBS). The authors are grateful to Dr. Gavin Arteel’s laboratory (University of Louisville) for the generous use of the LEICA cryostat for multicellular layer sections.

References

[1] Y. Gao, D.F. Katz, Multicompartmental pharmacokinetic model of tenofovir delivery by a vaginal gel, PLoS One 8 (9) (2013) e74404.
[2] A.M. Jarrett, et al., Sensitivity analysis of a pharmacokinetic model of vaginal anti-HIV microbicide drug delivery, J. Pharm. Sci. 105 (5) (2016) 1772–1778.
[3] D.C. Katz, M.N. Grote, T.D. Weaver, A mixed model for the relationship between climate and human cranial form, Am. J. Phys. Anthropol. 160 (4) (2016) 593–603.
[4] Y. Cu, W.M. Saltzman, Mathematical modeling of molecular diffusion through mucus, Adv. Drug Deliv. Rev. 61 (2) (2009) 101–114.
[5] B.C. Tang, et al., Biodegradable polymer nanoparticles that rapidly penetrate the human mucus barrier, Proc. Natl. Acad. Sci. USA 106 (46) (2009) 19268–19273.
[6] Q. Xu, et al., Impact of surface polyethylene glycol (PEG) density on biodegradable nanoparticle transport in mucus ex vivo and distribution in vivo, ACS Nano 9 (9) (2015) 9217–9227.
[7] M. Yang, et al., Biodegradable nanoparticles composed entirely of safe materials that rapidly penetrate human mucus, Angew. Chem. Int. Ed. Engl. 50 (11) (2011) 2597–2600.
[8] M. Yang, et al., Nanoparticle penetration of human cervicovaginal mucus: the effect of polyvinyl alcohol, J. Control Release 192 (2014) 202–208.
[9] Y. Gao, et al., Vaginal deployment and tenofovir delivery by microbicide gels, Drug Deliv. Transl. Res. 5 (3) (2015) 279–294.
[10] J. das Neves, et al., Polymer-based nanocarriers for vaginal drug delivery, Adv. Drug. Deliv. Rev. 92 (2015) 53–70.
[11] M.M. El-Hammadi, J.L. Arias, Nano-sized platforms for vaginal drug delivery, Curr. Pharm. Des. 21 (12) (2015) 1633–1644.
[12] D. Lembo, et al., Encapsulation of Acyclovir in new carboxylated cyclodextrin-based nanosponges improves the agent's antiviral efficacy, Int. J. Pharm. 443 (1–2) (2013) 262–272.
[13] Y.L. Traore, et al., Impact of hydroxychloroquine-loaded polyurethane intravaginal rings on lactobacilli, Antimicrob. Agents Chemother. 59 (12) (2015) 7680–7686.
[14] K.J. Whaley, et al., Novel approaches to vaginal delivery and safety of microbicides: biopharmaceuticals, nanoparticles, and vaccines, Antiviral Res. 88 (Suppl 1) (2010) S55–S66.
[15] L.M. Ensign, R. Cone, J. Hanes, Nanoparticle-based drug delivery to the vagina: a review, J. Control Release 190 (2014) 500–514.
[16] J.M. Steinbach, Protein and oligonucleotide delivery systems for vaginal microbicides against viral STIs, Cell Mol. Life Sci. 72 (3) (2015) 469–503.
[17] Y. Cu, W.M. Saltzman, Controlled surface modification with poly(ethylene)glycol enhances diffusion of PLGA nanoparticles in human cervical mucus, Mol. Pharm. 6 (1) (2009) 173–181.
[18] S.K. Lai, Y.Y. Wang, J. Hanes, Mucus-penetrating nanoparticles for drug and gene delivery to mucosal tissues, Adv. Drug Deliv. Rev. 61 (2) (2009) 158–171.
[19] C. Cunha-Reis, et al., Nanoparticles-in-film for the combined vaginal delivery of anti-HIV microbicide drugs, J. Control Release 243 (2016) 43–53.
[20] K.A. Woodrow, et al., Intravaginal gene silencing using biodegradable polymer nanoparticles densely loaded with small-interfering RNA, Nat. Mater. 8 (6) (2009) 526–533.
[21] Y. Cu, C.J. Booth, W.M. Saltzman, In vivo distribution of surface-modified PLGA nanoparticles following intravaginal delivery, J. Control. Release 156 (2) (2011) 258–264.
[22] L.M. Ensign, et al., Mucus-penetrating nanoparticles for vaginal drug delivery protect against herpes simplex virus, Sci. Transl. Med. 4 (138) (2012) p. 138ra79.
[23] L.M. Ensign, et al., Mucus penetrating nanoparticles: biophysical tool and method of drug and gene delivery, Adv. Mater. 24 (28) (2012) 3887–3894.
[24] S.K. Lai, et al., Rapid transport of large polymeric nanoparticles in fresh undiluted human mucus, Proc. Natl. Acad. Sci. USA 104 (5) (2007) 1482–1487.
[25] J.S. Suk, et al., PEGylation as a strategy for improving nanoparticle-based drug and

gene delivery, Adv. Drug Deliv. Rev. 99 (Pt A) (2016) 28–51.
[26] C.M. Caramella, et al., Mucoadhesive and thermogelling systems for vaginal drug delivery, Adv. Drug Deliv. Rev. 92 (2015) 39–52.
[27] J. das Neves, M. Amiji, B. Sarmento, Mucoadhesive nanosystems for vaginal microbicide development: friend or foe? Wiley Interdiscip. Rev. Nanomed. Nanobiotechnol. 3 (4) (2011) 389–399.
[28] T.W. Wong, M. Dhanawat, M.J. Rathbone, Vaginal drug delivery: strategies and concerns in polymeric nanoparticle development, Expert Opin. Drug Deliv. 11 (9) (2014) 1419–1434.
[29] Z. Li, et al., Transfer of IgG in the female genital tract by MHC class I-related neonatal Fc receptor (FcRn) confers protective immunity to vaginal infection, Proc. Natl. Acad. Sci. USA 108 (11) (2011) 4388–4393.
[30] K. Berginc, et al., Development and evaluation of an in vitro vaginal model for assessment of drug's biopharmaceutical properties: curcumin, AAPS PharmSciTech 13 (4) (2012) 1045–1053.
[31] M.A. Mirza, et al., A vaginal drug delivery model, Drug Deliv. 23 (8) (2016) 3123–3134.
[32] D.F. Katz, Y.J. Gao, S. Chang, Multi-compartmental transport of anti-HIV molecules into and through mucosa, Biophys. J . 102 (3) (2012) 594a.
[33] D.F. Katz, A. Yuan, Y.J. Gao, Vaginal drug distribution modeling, Adv. Drug Deliv. Rev. 92 (2015) 2–13.
[34] A.R. Geonnotti, D.F. Katz, Compartmental transport model of microbicide delivery by an intravaginal ring, J. Pharm. Sci. 99 (8) (2010) 3514–3521.
[35] M.E. Halwes, et al., Computational modeling of antiviral drug diffusion from poly (lactic- co-glycolic-acid) fibers and multicompartment pharmacokinetics for application to the female reproductive tract, Mol. Pharm. 15 (4) (2018) 1534–1547.
[36] K.K. Arien, G. Vanham, Y. Gali, A dual-chamber model of the female genital tract to evaluate epithelial toxicity of candidate anti-HIV microbicides, Curr. Protoc. Cell Biol. (2011) **Chapter 26**: p. Unit26 13.
[37] L. Cartwright, et al., In vitro placental model optimization for nanoparticle transport studies, Int. J. Nanomed. 7 (2012) 497–510.
[38] J. Gu, S. Yang, E.A. Ho, Biodegradable film for the targeted delivery of siRNA-loaded nanoparticles to vaginal immune cells, Mol. Pharm. 12 (8) (2015) 2889–2903.
[39] L.B. Sims, et al., Enhanced uptake and transport of PLGA-modified nanoparticles in cervical cancer, J. Nanobiotechnol. 14 (2016) 33.
[40] L.B. Sims, et al., Distribution of PLGA-modified nanoparticles in 3D cell culture models of hypo-vascularized tumor tissue, J. Nanobiotechnol. 15 (1) (2017) 67.
[41] M.G. Li, et al., Physiologically based pharmacokinetic modeling of PLGA nanoparticles with varied mPEG content, Int. J. Nanomed. 7 (2012) 1345–1356.
[42] M.G. Lu, et al., Physiologically based pharmacokinetic modeling of nanoparticles, Acs Nano 4 (11) (2010) 6303–6317.
[43] K. Maisel, et al., Nanoparticles coated with high molecular weight PEG penetrate mucus and provide uniform vaginal and colorectal distribution in vivo, Nanomedicine (Lond) 11 (11) (2016) 1337–1343.
[44] O. Mert, et al., A poly(ethylene glycol)-based surfactant for formulation of drug-loaded mucus penetrating particles, J. Control Release 157 (3) (2012) 455–460.
[45] T. Yu, et al., Biodegradable mucus-penetrating nanoparticles composed of diblock copolymers of polyethylene glycol and poly(lactic-co-glycolic acid). Drug Deliv. Transl. Res. (2012) 2(2).
[46] S. Eetezadi, et al., Effects of doxorubicin delivery systems and mild hyperthermia on tissue penetration in 3D cell culture models of ovarian cancer residual disease, Mol. Pharm. 12 (11) (2015) 3973–3985.
[47] C.G. England, et al., Enhanced penetration into 3D cell culture using two and three layered gold nanoparticles, Int. J. Nanomed. 8 (2013) 3603–3617.
[48] W. Gao, et al., Chemotherapeutic drug delivery to cancer cells using a combination of folate targeting and tumor microenvironment-sensitive polypeptides, Biomaterials 34 (16) (2013) 4137–4149.
[49] T.T.D. Le, et al., Evaluation of anti-HER2 scFv-conjugated PLGA-PEG nanoparticles on 3D tumor spheroids of BT474 and HCT116 cancer cells, Adv. Natural Sci.-Nanosci. Nanotechnol. 7 (2) (2016).
[50] S.K. Lai, et al., Nanoparticles reveal that human cervicovaginal mucus is riddled with pores larger than viruses, Proc. Natl. Acad. Sci. USA 107 (2) (2010) 598–603.
[51] J.M. Gamboa, K.W. Leong, In vitro and in vivo models for the study of oral delivery of nanoparticles, Adv. Drug Deliv. Rev. 65 (6) (2013) 800–810.
[52] L.M. Ensign, et al., Enhanced vaginal drug delivery through the use of hypotonic formulations that induce fluid uptake, Biomaterials 34 (28) (2014) 6922–6929.
[53] W. Gao, et al., Progress in siRNA delivery using multifunctional nanoparticles, Methods Mol. Biol. 629 (2010) 53–67.
[54] M. Mir, N. Ahmed, A.U. Rehman, Recent applications of PLGA based nanostructures in drug delivery, Colloids Surf. B Biointerfaces 159 (2017) 217–231.
[55] C. Salvador-Morales, et al., Recent developments in multifunctional hybrid nanoparticles: opportunities and challenges in cancer therapy, Front. Biosci. (Elite Ed) 4 (2012) 529–545.
[56] H. Cai, et al., Engineering PLGA nano-based systems through understanding the influence of nanoparticle properties and cell-penetrating peptides for cochlear drug delivery, Int. J. Pharm 532 (1) (2017) 55–65.
[57] C.J. Cheng, W.M. Saltzman, Enhanced siRNA delivery into cells by exploiting the synergy between targeting ligands and cell-penetrating peptides, Biomaterials 32 (26) (2011) 6194–6203.
[58] J. Zhou, et al., Octa-functional PLGA nanoparticles for targeted and efficient siRNA delivery to tumors, Biomaterials 33 (2) (2012) 583–591.
[59] A. Ediriwickrema, et al., Multi-layered nanoparticles for combination gene and drug delivery to tumors, Biomaterials 35 (34) (2014) 9343–9354.